

Article

Thermodynamic Origin of the Vitreous Transition

Robert Tournier F.

Centre National de la Recherche Scientifique, Université Joseph Fourier, Consortium de Recherches pour l'Émergence de Technologies Avancées, B.P. 166, 38042 Grenoble Cedex 09, France; E-Mail: Robert.Tournier@grenoble.cnrs.fr; Tel.: +33-608-716-878; Fax: +33-476-881-280

Received: 22 March 2011; in revised form: 19 April 2011 / Accepted: 5 May 2011 /

Published: 9 May 2011

Abstract: The vitreous transition is characterized by a freezing of atomic degrees of freedom at a temperature T_g depending on the heating and cooling rates. A kinetic origin is generally attributed to this phenomenon instead of a thermodynamic one which we develop here. Completed homogeneous nucleation laws reflecting the energy saving due to Fermi energy equalization of nascent crystals and their melt are used. They are applied to bulk metallic glasses and extended to inorganic glasses and polymers. A transition T_g^* among various T_g corresponds to a crystal homogeneous nucleation temperature, leading to a preliminary formation of a cluster distribution during the relaxation time preceding the long steady-state nucleation time of crystals in small samples. The thermally-activated energy barrier $\Delta G_{2l}^*/k_B T$ at T_g^* for homogeneous nucleation is nearly the same in all glass-forming melts and determined by similar values of viscosity and a thermally-activated diffusion barrier from melt to cluster. The glass transition T_g^* is a material constant and a linear function of the energy saving associated with charge transfers from nascent clusters to the melt. The vitreous transition and the melting temperatures alone are used to predict the free-volume disappearance temperature equal to the Vogel-Fulcher-Tammann temperature of fragile glass-forming melts, in agreement with many viscosity measurements. The reversible thermodynamic vitreous transition is determined by the disappearance temperature T_g^* of the fully-relaxed enthalpy H_r that is not time dependent; the observed specific heat jump at T_g^* is equal to the proportionality coefficient of H_r with $(T_g^* - T_a)$ for $T \leq T_g^*$ as expected from the enthalpy excess stored by a quenched undercooled melt at the annealing temperature T_a and relaxed towards an equilibrium vitreous state. However, the heat flux measurements found in literature over the last 50 years only gave an out-of-equilibrium T_g since the enthalpy is continuous at T_g^* without visible heat jump.

Keywords: 64.70 kj glasses; 64.70 P glass transitions; 64.70 pe metallic glasses; 64.70 ph. non metallic glasses; 64.70 pj polymers; 64.60 Q-nucleation

1. Introduction

The vitreous state is described, up to now, as a freezing of liquid-state below a temperature T_g called vitreous or glass transition, below which the viscosity becomes time dependent with values above 10^{12} – 10^{13} Pa.s. This transformation at T_g is also observed in the heat flow, measured with a technique of differential scanning calorimetry (DSC); endothermic and exothermic heats respectively, depending on the heating and the cooling rates, characterize glass-melt out-of-equilibrium transformations. The glass-forming melt viscosity follows a Vogel-Fulcher-Tammann (VFT) law diverging when the temperature tends to T_0 ; T_0 is much smaller than T_g and called the ideal glass transition temperature [1-3]. Recent work has shown that the size of heterogeneous regions simultaneously moving to allow a viscous flow grows in the vicinity of the glass transition [4]. The heterogeneous dynamics could also be the result of critical-like fluctuations of static structural order, characterized by a static correlation length diverging towards the ideal glass-transition point T_0 in the absence of a thermodynamic transition at T_g . Two glass transition temperatures T_0 and T_g could exist without any connection between the two [5]. In addition, the residual entropy available in undercooled melt, as compared to the crystal one at the glass transition, varies strongly among glasses. The Kauzmann temperature T_k has been defined as the temperature at which the crystal fusion entropy would be consumed upon cooling. It could also lead, at thermodynamic equilibrium, to a hidden phase transition following several speculations found in literature [1,2,6].

The high temperature viscosity of some polymer melts, including measurements above the melting point, follows a VFT scaling law giving $T_0 = T_{01} = 0.77 \times T_g$ [7]. In the vicinity of the glass transition, the enthalpy relaxation times or the viscosity gives a value $T_0 = T_{02}$ smaller than T_{01} . Therefore, if T_0 increases above T_g within a narrow range of temperature, it explains why the viscosity values measured at high temperatures do not determine the ideal glass transition. The change of T_0 occurs around the temperature T_s where a break is seen in some volume-*versus*-temperature plots [8]. Many experimental results tend to prove that the ideal glass transition temperature is equal to T_{02} with a viscosity close to T_g following a VFT law with $T_0 = T_{02}$ [3]. The viscosity is an exponential function of $B/(T - T_0)$ with B nearly proportional to $(T_g - T_0)$ [9].

Following Doolittle's and Ramachandrarao and Dubey's works, the free-volume of glass-forming melts would disappear at the ideal glass transition temperature T_0 [10,11]; then, the two free-volume disappearance temperatures T_{0g} and T_{0m} correspond respectively to our two VFT temperatures T_{02} and T_{01} respectively. Recent numerical simulations of critical-like behavior of glass-forming melts down to T_0 (assuming that the glass transition only corresponds to a slowing-down of dynamics) suggests that the melt entropy excess at equilibrium must tend to zero for $T = T_{02} = T_{0g}$ instead of $T = T_k$, T_k being the Kauzmann temperature [5,6,12]. New universal and coherent relations between T_g , $T_{0g} = T_{02}$ and $T_{0m} = T_{01}$ are proposed in this paper and checked for a series of data in real systems. The associated predictions still need to be clarified.

The vitreous transition, observed by DSC techniques in undercooled melts, is generally time dependent and not strictly reversible, because using the same cooling and heating rates do not lead to the same transformation temperature [13]. These properties underline the kinetic aspects of the transition. A rapid cooling at temperatures far below T_g followed by an annealing as a function of time at a temperature $T_a < T_g$ induces an enthalpy relaxation, saturating to a value H_r ; H_r itself tends to zero for the transition temperature T_g^* . From published values of H_r , it is shown that the reversible transition occurs at T_g^* , and that the transformation into the vitreous state is postponed by quenching the undercooled melt. It is achieved after a time lag equal to the relaxation time by annealing at $T = T_a$. Some DSC techniques are able to separate the specific heat at T_g^* in two parts; the temperature dependent one is reversible and attached to the thermodynamic aspect of the transition, and the time dependent “irreversible” one is attached to the kinetic aspect. The reversible specific heat jump temperature measured by this technique does not depend on cooling and heating rates and is only a function of the chemical composition [13].

In this paper, we show that crystal homogeneous nucleation occurs at the glass transition T_g^* of fragile glass-forming melts without any adjustable parameter. This nucleation only depends on the melt composition, and the obtained frozen state is a preliminary step on the long way leading to crystallization. The free energy change associated with a crystal formation in a melt has been accepted for many years, and, regardless of its radius, as if it had the same state equation as a solid outside the melt, which does not reflect the fact that the Fermi energy of a nascent crystal in a metallic melt becomes equal to that of the melt. In order to determine why the vitreous state replaces the crystallized state, a “volume energy saving” ε_v has been added to the Gibbs free-energy change associated with crystal homogeneous nucleation in melt, to obtain the equalization of Fermi energies transferring free electrons from the crystal to the melt [14-16]. The energy saving ε_v is equal to $\varepsilon_{lps}\Delta H_m/V_m$, ΔH_m , V_m , and ε_{lps} respectively being the molar fusion heat, the molar volume, and the energy saving coefficient, where ε_{lps} is a numerical coefficient depending on the reduced temperature $\theta = (T - T_m)/T_m$ [16]. The indexes *s* and *l* are related to solid and liquid states. The index *p* is suppressed for unmelted crystals acting as growth nuclei and replaced by the index *g* for crystals resulting from homogeneous nucleation in glass-forming melts. The value of ε_{lps} can be predicted using the VFT temperatures T_{01} and T_{02} viewed as the disappearance temperatures T_{0g} and T_{0m} of fragile-glass-forming melt free-volume and of Fermi energy difference between crystal and melt [14,15]. The vitreous transition T_g^* only depends on the energy saving coefficient. The experimental values of T_{0g} can also be used to predict the vitreous transition temperature T_g^* .

In this model, the crystal growth starts at the crystal nucleation temperature with a cluster preliminary formation on the long way leading to crystallization. It is locked at the vitreous transition by a freezing without any change of enthalpy and entropy. The same analysis is successfully applied to some polymers and non-metallic glass-formers. The presence of a similar “volume energy saving”, governing the vitreous transition, is determined. This phenomenon is probably due to a free energy which depends on the number of molecules or atoms in a small crystal having a noncritical radius or to an electrostatic interaction between uncompensated average charges proportional to $n^{1/2}$ carried by nascent crystals built from a random distribution of ions on various sub-lattices and screened by ionic charges of the melt.

This paper is built as follows: Section 2. Model; 2.1. New equations governing the crystal nucleation; 2.2. The ideal glass transition T_0 and the energy saving associated with crystal formation; Section 3. Review of experimental results and discussion; 3.1 Presentation of Table 1 and Figure 1; 3.2. Homogeneous nucleation time of crystals and relaxation time; 3.3. The thermodynamic vitreous transition T_g^* at the disappearance temperature of the fully-relaxed enthalpy; 3.4. The crystal homogeneous nucleation temperature at T_g^* ; 3.5. Volume energy saving associated with nascent crystals in non-metallic glass-forming melts; 3.6. Thermodynamic origin of the relaxed enthalpy and out-of-equilibrium transition temperatures T_g ; Section 4. Summary and complementary information on the two crystal nucleation temperatures; Section 5. Conclusions.

2. Model

2.1. New Equations Governing the Crystal Nucleation

The classical equation describing the Gibbs free-energy change associated with a crystal formation, predicts the absence of surviving crystals above the melting temperature T_m [17]. On the contrary, their existence is predicted far above T_m if an energy saving per volume unit $\varepsilon_v = \varepsilon_{lps} \times \Delta H_m/V_m$ is added. The maximum undercooling ratio $\theta_1 = (T_1 - T_m)/T_m$ is observed as being of the order of -0.2 in liquid elements using droplet sizes of 50–10,000 micrometers instead of $-2/3$ [18]. This pseudo-maximum has until now been considered to be the maximum of the homogeneous nucleation rate in contradiction with a detailed study of crystallization temperature of gallium droplets as a function of their diameter. Two undercooling temperature dwells, instead of one, corresponding to $\theta_1 = -0.28$ and $\theta_1 = -0.5$ have been observed for diameters varying from 1 to 1,000 micrometers [19]. This phenomenon is induced by a distribution of surviving crystal radii between two boundary radii after overheating. A large overheating rate has to be applied in order to melt a part of them and obtain an undercooling rate dwell of about -0.2 [20]. The second dwell corresponding to stronger undercooling rates, is due to numerous surviving crystals having the smallest radius [21–23]. The sample radius has to be strongly reduced to observe it. The energy saving ε_v depends on the Fermi energy difference between solid and liquid and is an even function of the reduced temperature $\theta = (T - T_m)/T_m$ as shown in (1) [14,16]:

$$\varepsilon_v = \varepsilon_{lps} \frac{\Delta H_m}{V_m} = \varepsilon_{lps0} \left(1 - \frac{\theta^2}{\theta_{0lps}^2}\right) \frac{\Delta H_m}{V_m} \quad (1)$$

Consequently, the fusion heat of unmelted crystals remains equal to ΔH_m regardless of their radius, because $d\varepsilon_{ls}/d\theta = 0$ and $d(\Delta G_{2ls}^*)/d\theta = \Delta H_m \times 4\pi R^3/3/V_m$ at $\theta = 0$, with ΔG_{2ls}^* being the completed Gibbs free energy change for a crystal formation in a melt given by (2):

$$\Delta G_{2lps}(R, \theta) = \frac{\Delta H_m}{V_m} (\theta - \varepsilon_{lps}) 4\pi \frac{R^3}{3} + 4\pi R^2 \frac{\Delta H_m}{V_m} (1 + \varepsilon_{lps}) \left(\frac{12k_B V_m \ln K_{ls}}{432\pi \times \Delta S_m}\right)^{1/3} \quad (2)$$

k_B being the Boltzmann constant, ΔS_m the fusion entropy per mole and $\ln K_{lps}$ given by (12). The volume energy saving ε_v is added to the classical Gibbs free energy $\theta \times \Delta H_m/V_m$ and the surface energy is modified by the factor $(1 + \varepsilon_{ls})$. The classical equation $\Delta G_{1ls}(\theta)$ is deduced from (2) with $\varepsilon_{ls} = 0$ [17–19]. The experimental values of surface energy and lowest undercooling temperatures of many liquid elements have been used to determine the new surface energy and ε_{ls} in (1,2) [17]. This

Equation (2) allows us to calculate the unique homogeneous nucleation temperature $\theta_{2ls} = -2/3$ and the crystallization temperatures of liquid elements from intrinsic growth nuclei without any adjustable parameter [21-23].

The energy saving becomes equal to zero at T_m above a radius a little larger than the critical radius for crystal growth nucleation to obey, at equilibrium, the classical J. W. Gibbs's phase coexistence rule and because a free electron cannot be transferred from the crystal to the melt with an energy saving larger than the Fermi energy. The crystal homogeneous nucleation maximum-rate temperature T_{2lps} (or θ_{2lps}) defined by (3) in the undercooled melt is respectively called θ_{2lgs} or θ_{2ls} with values of ε_{lps0} equal to ε_{lgs0} or ε_{ls0} :

$$\theta_{2lps} = \frac{\varepsilon_{lps} - 2}{3} \quad (3)$$

The θ_{2lps} only depends on the coefficient ε_{lps} defined by (1) and (3) and does not depend on other material properties. It is equal to $(T_{olps} - T_m)/T_m$ where T_{olps} is equal to T_{om} or T_{og} . The critical energy barrier, the critical radius and θ_{2lps} given by (3) have been calculated assuming that ε_{lps} is not radius dependent. This assumption works because the influence of $d\varepsilon_{lps}/dR$ is negligible on the critical parameters of a lot of melts. Equations (1-3) have already been used to predict the time-temperature-transformation diagrams of $Mg_{65}Y_{10}Cu_{25}$, $Zr_{41.2}Ti_{13.8}Cu_{12.5}Ni_{10}Be_{22.5}$ and $Pd_{43}Cu_{27}Ni_{10}P_{20}$ melts [14,15] and the undercooling temperature dwells of liquid elements, in agreement with the experiments without using any adjustable parameter [21-23]. Unequal coefficients $\varepsilon_{ls} \neq \varepsilon_{lgs}$ would lead to $\theta_{2ls} \neq \theta_{2lgs}$. Equal coefficients $\varepsilon_{lps} = \varepsilon_{ls} = \varepsilon_{lgs}$ would lead to the same homogeneous nucleation temperature; the glass transition would be equal to the crystallization temperature.

2.2. The Ideal Glass Transition Temperature T_0 and The Energy Saving Associated with Crystal Formation

Many experiments show the presence of numerous intrinsic growth nuclei in melts. Glasses can give rise to about 10^{25} nanocrystals per m^3 within a few hours when they are annealed above the vitreous transition. This number is much too large to be compared with the classical homogeneous nucleation rate. High resolution microscopy reveals the existence of "mean range order" clusters called MRO with a radius of about one nanometer in amorphous $Fe_{83}B_{17}$ [24]. These entities are not viewed as surviving crystals because they do not exist in the literature. They are as numerous as the nanocrystals and could be growth nuclei. A recent observation of an irreversible viscosity of $Fe_{85}B_{15}$ far above the liquidus temperature could also be a sign of the existence of surviving crystals up to temperatures as high as $1.3 T_m$ [25].

A liquid-solid transition is accompanied by Fermi energy and volume changes in metallic glass-forming melts. The free volume change ΔV and the Fermi energy difference ΔE_F are expected to disappear at the same reduced temperature $\theta_{olps} > -2/3$ and to be maximum at the melting temperature ($\theta = 0$) in agreement with the thermal variation given by (1) of the energy saving coefficient ε_{lps} of liquid elements between $\theta_{olps} = \theta_{2lps} \cong -2/3$ and $\theta = 0$ [14-16].

The glass-forming melt viscosity is represented by a VFT relation given by (4) depending on three parameters η_0 , B and T_0 , in the region of the glass transition T_g [1-3]. Its variation by several orders of

magnitude above and close to T_g is used to determine T_0 [3,26] because including viscosity values measured far above the melting temperature increases the T_0 value [27,28]; it is important to fix $\eta_0 \cong N_A \times h/V_m$ with N_A Avogadro's number, h Planck's constant and V_m the molar volume to evaluate T_0 and B in (4) [28]:

$$\eta = \eta_0 \exp\left(\frac{B}{T - T_0}\right) \quad (4)$$

The relaxation time dependence in the temperature range between the onset and the end of the endothermic transition is observed by DSC. At a constant heating rate, the relaxation time τ is also described by the VFT-type relation (5):

$$\tau = \tau_0 \exp\left(\frac{B}{T - T_0}\right) \quad (5)$$

T_0 and B are determined using a pre-exponential coefficient τ_0 of about 10^{-14} s [3,27,28].

The free-volume of glass-forming melts is a linear function of $(T - T_0)$. Doolittle's relation introduces the free volume in the exponential of (4,5) [10]; ΔV would be equal to zero for $T = T_0$ in the absence of vitreous transition. The values of T_0 would correspond to the extrapolated free-volume disappearance temperature. Some measurements exist [29,30]. For example, the $\text{Pd}_{43}\text{Cu}_{27}\text{Ni}_{10}\text{P}_{20}$ volume in the liquid and solid states are known down to an extrapolated value $\Delta V = 0$ occurring for $T_{02} \cong 452$ K. In $\text{Pd}_{40}\text{Cu}_{30}\text{Ni}_{10}\text{P}_{20}$, the VFT law leads to $T_{02} = 447$ K [31].

The minimum value of ε_{lps0} in undercooled melt can be calculated only knowing T_{01} (or θ_{01}) and T_{02} (or θ_{02}) from VFT equations [14,15]. The quadratic equation (6) is obtained applying (1) and (3) for $\theta = \theta_{2lps}$:

$$\frac{\theta_{2lps}^2 \varepsilon_{lps0}}{\theta_{0lps}^2} + 3\theta_{2lps} + 2 - \varepsilon_{lps0} = 0 \quad (6)$$

There are two solutions for θ_{2lps} when ε_{lps0} is larger than a minimum value as already described [14,15]. The relations (7) and (8) between ε_{lps0} , θ_{2lps} and θ_{0lps}^2 are respected when the double solution corresponds to a minimum value of ε_{lps0} larger than 1. It is given by (7,8) and occurs when $9 - 4 \times (2 - \varepsilon_{lps0}) \times \varepsilon_{lps0} / \theta_{0lps}^2 = 0$:

$$\varepsilon_{lps0} = \varepsilon_{lps}(\theta = 0) = 1.5 \times \theta_{2lps} + 2 \quad (7)$$

$$\theta_{0lps}^2 = \frac{8}{9} \varepsilon_{lps0} - \frac{4}{9} \varepsilon_{lps0}^2 \quad (8)$$

The knowledge of θ_{02} and θ_{01} from VFT equations chosen respectively equal to θ_{0lgs} and θ_{0ls} and the use of (7) or (8) determine ε_{lps0} and θ_{2lps} and the minimum value of ε_{lps0} . The existence of two glass-former classes and their boundaries are predicted completing Angel's description, if we assume that $\theta_{2lgs} = \theta_g^* = (T_g^* - T_m)/T_m$ [3].

Fragile bulk glasses correspond to $\theta_{0lgs} = \theta_{0g} > -2/3$ and $\varepsilon_{lgs0} > 1$, and fragile and quenched glasses to $\varepsilon_{lgs0} < 1$ and $\theta_{2lgs} = \theta_{0g} = -2/3$. The undercooled liquid state can be recovered by heating the glass above T_{2lgs} (or θ_{2lgs}) because the condition $\varepsilon_{lgs0} > 1$ stabilizes it. It is not recovered when $\varepsilon_{lgs0} < 1$ and $\theta_{0g} = -2/3$ because there is no minimum value of ε_{lgs0} . All predictions of (7,8) are related to the

free-volume disappearance temperature of fragile undercooled melts which is equal to the ideal glass transition temperature. Angel's classification does not fix a quantified boundary between strong and fragile ones.

The strong glass-forming melts correspond to $\theta_{0lgs} \leq -2/3$, $\varepsilon_{lgs0} < 2$, and $\theta_{2lgs} > -2/3$. They also have a viscosity larger than fragile melts with temperature dependence close to Arrhenius law. Their vitreous transition temperature can be a very large fraction of the melting temperature. The largest value of ε_{lps0} is deduced from the experimental values of θ_{0lps} and θ_{2lps} using (6). Strong glass-forming melts have a homogeneous nucleation temperature always larger than $T_m/3$ without metastable values of ε_{lps0} regardless of the energy saving.

3. Review of Experimental Results and Discussion

3.1. Presentation of Table 1 and Figure 1

The melting temperatures T_m , the experimental glass transition temperatures T_g or $\theta_g = (T_g - T_m)/T_m$, the VFT temperatures T_{01} determined up to temperatures much higher than T_g , the VFT temperatures T_{02} determined by viscosity or relaxation time measurements in the vicinity of T_m , the free-volume disappearance temperatures $T_{0g} = T_{0lgs}$ calculated using (7,8) and (18) considering that T_g is, in a first approximation, nearly equal to the thermodynamic glass nucleation temperature T_g^* , the saving energy coefficients $\varepsilon_{ls0}(\theta = 0)$ of crystals surviving in the melt far above T_g calculated using (19), the saving energy coefficients $\varepsilon_{lgs0}(\theta = 0)$ of nascent crystals homogeneously nucleated in the melt near T_g calculated using (18), the free-volume disappearance temperatures $T_{0m} = T_{01}$ calculated using (7,8,19,20), T_g , and the references [32-63] are given in Table 1.

Properties of 20 non-metallic glasses and polymers are numbered with references. B_2O_3 is numbered 11 and 12. Two values of T_g are used. This glass is not easily crystallized. It gives rise to two crystallographic structures and its highest melting temperature is 783 K. SiO_2 N³ is a strong glass ($\theta_{01} < -0.666$). Hevea rubber N⁵⁰ is just at the limit separating strong glasses from fragile ones because T_{0g} is a little larger than $T_m/3$.

Properties of 28 bulk metallic glasses are used and numbered with references. The difference of liquidus and solidus temperatures is sometimes too large. A homogeneous melt has a well-defined Fermi energy. The melting temperature has been chosen between these two limits looking at the DSC profile. Two melting temperatures $T_m = 728$ K and $T_1 = 925$ K are used for $La_{55}Al_{25}Ni_{20}$ N²¹ and 22. The first one corresponds to the largest endothermic peak and the second one to the liquidus. We find $\varepsilon_{ls0} = 1.65$ and about 1.51 respectively. Two melting temperatures are also used for $Pd_{40}Ni_{40}P_{20}$ N²⁴ and 25, $T_m = 987$ K and $T_m = 884$ K leading to $\varepsilon_{ls0} = 1.63$ and 1.56 respectively. The melting temperatures of $La_{55}Al_{25}Ni_5Cu_{15}$ N²⁸, $La_{55}Al_{25}Ni_{15}Cu_5$ N³² and $La_{55}Al_{25}Ni_5Cu_{10}Co_5$ N⁴¹ are respectively chosen equal to 700 K instead of 878 K, 729 K instead of 899 K and 754 K instead of 822.5 K.

Experimentalists call all glasses characterized by a crystallization temperature T_x occurring near T_g "conventional". Among them, glasses have a value of T_g close to $T_m/2$. The glass transitions of $Al_{87}Co_4Ce_9$, $Al_{87}Co_6Ce_7$, $Al_{87}Co_8Ce_5$, $Al_{85}Co_{10}Ce_5$ and $Al_{90}Co_5Ce_5$ are not reported because they cannot be distinguished from the crystallization temperature T_x , in the absence of endothermic heat before crystallization in a DSC run [62]. The values of $\theta_x = (T_x - T_m)/T_m$ are respectively equal to

−0.481, −0.523, −0.533, −0.543, −0.567. $\text{Au}_{0.77}\text{Ge}_{0.136}\text{Si}_{0.094}$ N 51 is characterized by a crystallization temperature T_x occurring above and very close to T_g with $\theta_g = -0.539$ [63]. All these alloys have an energy saving coefficient larger than 1. They could belong to the fragile glass class because they have a VFT temperature T_0 larger than $T_m/3$.

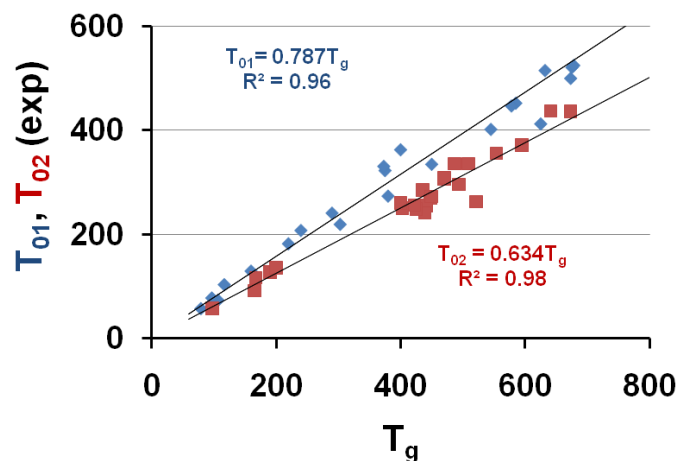
Table 1. Some properties of 46 glass-forming melts are presented: T_m the melting temperature; T_g the vitreous transition temperature, $\theta_g = (T_g - T_m)/T_m$, T_{01} and T_{02} the Vogel-Fulcher-Tammann temperatures, as found in various references; T_{0g} the free-volume disappearance temperature calculated from T_g and not from T_g^* ; ϵ_{ls0} the energy saving coefficient of tiny crystals surviving in the melt and acting as growth nuclei; ϵ_{lgs0} the energy saving coefficient of homogeneously-nucleated crystals in the melt; ϵ_{ls0} and ϵ_{lgs0} being used to calculate T_{0m} and T_{0g} ; T_{0m} the free-volume disappearance temperature also calculated from T_g and not from T_g^* ; and references.

	Glass	T_m	T_g	θ_g	T_{01}	T_{02}	T_{0g}	ϵ_{ls0}	ϵ_{lgs0}	T_{0m}	References
1	As_2S_3	585	481	−0.178		270	319	1.822	1.732	363	[32,33]
2	Propylene glycol	214	167	−0.220		117	108	1.780	1.671	125	[26,34,35]
3	SiO_2	1,993	1,473	−0.261		300			1.36		[2,36]
4	Propylene carbonate	217	160	−0.263	130		102	1.737	1.606	119	[35]
5	polystyrene	513	375	−0.269	323		239	1.731	1.596	280	[26,37]
6	$\text{Pd}_{43}\text{Ni}_{10}\text{Cu}_{27}\text{P}_{20}$	802	585	−0.271	452		372	1.729	1.594	436	[29,38,39]
7	O-Terphenil	329	240	−0.271	208		153	1.729	1.593	179	[3,26,40]
8	$\text{Pd}_{40}\text{Cu}_{30}\text{Ni}_{10}\text{P}_{20}$	823	578	−0.298	447		366	1.702	1.553	432	[29,31,39]
9	Salol	315	220	−0.302	183		139	1.698	1.548	165	[3,26,35]
10	As_2Se_3	645	450	−0.302	335		285	1.698	1.547	337	[41]
11	B_2O_3	783	545	−0.304	402		345	1.696	1.544	408	[3,11,32]
12	B_2O_3	783	521	−0.335		263	330	1.665	1.498	393	[3,11,32]
13	Bromopentane	158	107	−0.323	74		68	1.677	1.516	80	[26]
14	ZnCl_2	565	380	−0.327	274		241	1.673	1.509	286	[2,26]
15	Butene 1	88	59	−0.330			37	1.670	1.506	44	[2]
16	$\text{Zr}_{41.2}\text{Ti}_{13.8}\text{Cu}_{12.5}\text{Ni}_{10}\text{Be}_{22.5}$	937	625	−0.333	413		396	1.667	1.501	472	[39,42]
17	$\text{La}_{55}\text{Al}_{25}\text{Ni}_{10}\text{Cu}_{10}$	662	441	−0.334		255	280	1.666	1.499	333	[43-45]
18	2 Methylpentane	120	80	−0.338	58		50	1.663	1.494	60	[2,26,46]
19	Toluene	178	117	−0.343	104		74	1.657	1.485	89	[47]
20	Glycerol	293	190	−0.352		128	121	1.648	1.473	144	[26,34,35]
21	$\text{La}_{55}\text{Al}_{25}\text{Ni}_{20}$	728	470	−0.354		307	299	1.646	1.469	358	[43-45]
22	$\text{La}_{55}\text{Al}_{25}\text{Ni}_{20}$	925	470	−0.492		309	330	1.508	1.262	394	[43-45]
23	PET = $(\text{C}_{10}\text{H}_8\text{O}_4)_n$	542	342	−0.369			219	1.631	1.446	262	[2]
24	$\text{Pd}_{40}\text{Ni}_{40}\text{P}_{20}$	884	554	−0.373		356	355	1.627	1.440	425	[48,49]
25	$\text{Pd}_{40}\text{Ni}_{40}\text{P}_{20}$	987	554	−0.439		356	369	1.561	1.342	442	[48,49]
26	$\text{Pt}_{57.5}\text{Cu}_{14.7}\text{Ni}_{5.3}\text{P}_{22.5}$	813	509	−0.374		336	326	1.626	1.439	390	[50]
27	$\text{Pd}_{0.775}\text{Cu}_{0.06}\text{Si}_{0.165}$	1,015	632	−0.377	515		405	1.623	1.434	486	[51]
28	$\text{La}_{55}\text{Al}_{25}\text{Ni}_5\text{Cu}_{15}$	700	436	−0.378		286	279	1.622	1.433	335	[43-45]
29	$\text{Zr}_{52.5}\text{Cu}_{17.9}\text{Ni}_{14.6}\text{Al}_{10}\text{Ti}_5$	1,090	675	−0.381	521		434	1.619	1.429	519	[52]

Table 1. Cont.

	Glass	T_m	T_g	θ_g	T_{01}	T_{02}	T_{0g}	ϵ_{is0}	ϵ_{igs0}	T_{0m}	References
30	Pt _{57.3} Cu _{14.6} Ni _{5.3} P _{22.8}	788	487	-0.382		336	313	1.618	1.427	375	[50]
31	Se	491	303	-0.383	220		195	1.617	1.426	233	[2,53]
32	La ₅₅ Al ₂₅ Ni ₁₅ Cu ₅	729	449	-0.384		273	289	1.616	1.424	346	[43-45]
33	Au ₄₉ Ag _{5.5} Pd _{2.3} Cu _{26.9} Si _{16.3}	655	403	-0.385		250	259	1.615	1.423	311	[39]
34	Ethanol	159	97	-0.390	78	58	63	1.610	1.415	75	[2,11,32]
35	Zr _{58.5} Cu _{15.6} Ni _{12.8} Al _{10.3} Nb _{2.8}	1,110	673	-0.394		437	435	1.606	1.409	522	[54]
36	Zr ₅₇ Cu _{15.4} Ni _{12.6} Al _{10.3} Nb ₅	1,120	678	-0.395	525		438	1.605	1.408	526	[52]
37	Pr ₅₅ Ni ₂₅ Al ₂₀	820	494	-0.398		296	320	1.602	1.404	384	[55]
38	Ti _{41.5} Cu _{37.5} Ni _{7.5} Zr _{2.5} Hf ₅ Sn ₅ Si ₁	1,176	693	-0.411			452	1.589	1.384	543	[56]
39	Cu ₄₇ Ti ₃₄ Zr ₁₁ Ni ₈	1,144	673	-0.412	500		439	1.588	1.382	527	[57]
40	Y ₅₆ Al ₂₄ Co ₂₀	1,085	636	-0.414	614		416	1.586	1.379	499	[58]
41	La ₅₅ Al ₂₅ Ni ₅ Cu ₁₀ Co ₅	754	439	-0.418		241	288	1.582	1.374	345	[43-45]
42	Mg _{59.5} Cu _{22.9} Ag _{6.6} Gd ₁₁	734	425	-0.421		249	279	1.579	1.369	335	[59]
43	Mg ₆₁ Cu ₂₈ Gd ₁₁	737	422	-0.427		256	278	1.573	1.359	334	[59]
44	Mg ₆₅ Cu ₂₅ Y ₁₀	739	400	-0.459	363	260	271	1.541	1.312	325	[27]
45	Zr _{46.75} Ti _{8.25} Cu _{7.5} Ni ₁₀ Be _{27.5}	1,070	595	-0.444		372	398	1.556	1.334	477	[60]
46	Cyclo-octanol	298	165	-0.446		92	110	1.554	1.331	133	[26]
47	Zr ₆₅ Al ₁₀ Ni ₁₀ Cu ₁₅	1,161	641	-0.448		437	430	1.552	1.328	516	[39]
48	Ce ₆₀ Al ₁₀ Ni ₁₀ Cu ₂₀	677	373	-0.449	331		250	1.551	1.326	300	[61]
49	Al ₈₇ Co ₄ Ce ₉	1,104	573	-0.481			397	1.519	1.279	475	[62]
50	Hevea rubber	421	200	-0.525		136	147	1.475	1.213	174	[32]
51	Au _{0.77} Ge _{0.136} Si _{0.094}	629	290	-0.539	241		217	1.461	1.192	257	[63]

Figure 1. The VFT temperatures T_{01} and T_{02} given in Table 1 are plotted *versus* T_g ; T_{02} corresponds to measurements in the vicinity of T_g and T_{01} includes viscosity measurements at higher temperatures. $T_{01} \cong 0.787 T_g$ and $T_{02} \cong 0.634 T_g$.



The temperatures T_{01} and T_{02} are plotted as a function of the vitreous transition temperature T_g in Figure 1; the upper straight line uses the equation $T_{01} = 0.787 \times T_g$ and corresponds to a similar law $T_{01} = 0.77 \times T_g$ already observed for 7 other polymers [7,64]; the lower straight line uses the equation $T_{02} = 0.634 \times T_g$.

3.2. Homogeneous Nucleation Temperature of Vitreous Phase and Relaxation Time

The calculation of the crystal nucleation full time t includes not only the steady-state nucleation time t_{sn} defined by $v \times t_{sn} = 1$ in (10) at the nucleation temperature, but also the time lag τ^{ns} in crystal transient nucleation defined by (9) [2] with K_{lgs} defined by (12):

$$\tau^{ns} = \frac{a_0^*}{2\pi K_{lgs}} \quad (9)$$

$$\ln(Jvt_{sn}) = \ln(K_{lgs} vt_{sn}) - \frac{\Delta G_{2lgs}^*}{k_B T} \quad (10)$$

$$J\tau^{ns} = \frac{\pi N}{12\Gamma} \exp\left(-\frac{\Delta G_{2lgs}^*}{k_B T}\right) \quad (11)$$

$$\ln(K_{lgs}) = \ln\left(\frac{A\eta_0}{\eta}\right) = (\ln A) \pm 2 - \frac{B}{(T - T_{0g})} \quad (12)$$

The steady-state nucleation rate is J , the volume sample v , Zeldovitch's factor Γ , the critical energy barrier $\Delta G_{2lgs}^*/k_B T$, $a_0^* = \pi^2/6$, the atom or molecule number per volume unit N . The quantity $\ln K_{lgs}$ is equal to $\ln A \cong 90 \pm 2$ for liquid elements in a broad temperature scale; $\ln A$ is a little smaller for crystallization of glass-forming melts. In the vicinity of T_g^* , and assuming that T_g^* (or θ_g^*) is equal to a crystal homogeneous nucleation temperature T_{2lgs} (or θ_{2lgs}), when $J = 1$, the crystal transient nucleation time τ^{ns} viewed as the relaxation time, can be calculated with (15) using the critical parameters (13) and (14):

$$\frac{\Delta G_{2lgs}^*}{k_B T} = \frac{12(1 + \varepsilon_{lgs})^3 \ln K_{lgs}}{81(\theta - \varepsilon_{lgs})^2(1 + \theta)} \quad (13)$$

$$R_{2ls}^*(\theta) = \frac{-2(1 + \varepsilon_{lgs})}{\theta - \varepsilon_{lgs}} \left(\frac{V_m}{N_A}\right)^{1/3} \left(\frac{12k_B V_m \ln K_{lgs}}{432\pi \times \Delta S_m}\right)^{1/3} \quad (14)$$

$$\tau^{ns} = \frac{\pi N}{12\Gamma} \exp(-\ln K_{lgs}) = \frac{\pi N}{12\Gamma} \exp(-\ln A_g) \times \exp\left(\frac{B}{T - T_{0g}}\right) = \tau_0 \exp\left(\frac{B}{T - T_{0g}}\right) \quad (15)$$

The coefficient of $\ln K_{lgs}$ in (13) is equal to 1 for $\theta = \theta_{2lgs} = (\varepsilon_{ls} - 2)/3$ when the crystal-steady-state nucleation time is minimum. The A_g is the A value defined by (12) at the glass transition, which is used for the homogeneously-nucleated cluster formation. Zeldovitch's factor given by (16) is calculated below, as a function of the number J_c of molecules or atoms in a spherical crystal of critical radius R_{2lgs}^* , given by (14) at $\theta_{2lgs} = \theta_g^*$. The pre-exponential time τ_0 given by (17) depends on A_g and $\ln(\tau^{ns}/\tau_0)$ is equal to $B/(T_g^* - T_{0g}) \cong 36.5 - 39$ at T_g^* [3,9]:

$$\Gamma = \left(\frac{\ln K_{lgs}}{3\pi}\right)^{1/2} \frac{1}{J_c} = \left(\frac{\ln K_{lgs}}{3\pi}\right)^{1/2} \frac{27}{8} \frac{\Delta S_m (\theta_{2lgs} - \varepsilon_{lgs})^3}{N_A k_B (1 + \varepsilon_{lgs})^3 \ln K_{lgs}} \quad (16)$$

$$\tau_0 = \frac{\pi N_A k_B (3\pi)^{1/2}}{6} \frac{N_A}{V_m} \frac{(1 + \theta_{2lgs})(\ln K_{lgs})^{1/2}}{\Delta S_m A_g} \quad (17)$$

where ΔS_m is the fusion entropy per mole, N_A the Avogadro number, θ_{2lgs} defined by (3), $N_A k_B = 8.32$ Joule. The temperature T_{2lgs} (or θ_{2lgs}) is a constant of the material and a unique function of

the energy saving ε_{lgs} in (3). It does not strictly depend on viscosity. Nevertheless, the viscosity has a strong influence on the occurrence of the maximum nucleation rate temperature because the critical energy barrier $\Delta G^*_{2lgs}/k_B T$ is proportional to $\ln K_{lgs}$ and the numerical coefficient of $\ln K_{lgs}$ in $\Delta G^*_{2lgs}/k_B T$ is equal to about 1 in a broad window of temperatures above T^*_g . The critical energy barrier $\Delta G^*_{2lgs}/k_B T$ is nearly the same at T^*_g for all glass-forming melts and $\ln K_{lgs}$ decreases with the increase in viscosity. The nucleation rate is at a maximum when $\ln K_{lgs}$ becomes exactly equal to $\Delta G^*_{2lgs}/k_B T_g$. This event occurs at T^*_g (or θ^*_g) = T_{2lgs} (or θ_{2ls}) for similar viscosity values because τ_0 , and the relaxation time τ_g^{ns} are nearly the same in all glass-forming melts at T_g .

The relaxation time τ_g^{ns} is generally of the order of 100 s at T_g . A value $\tau_0 = 1.4 \times 10^{-14}$ s is deduced with $B/(T_g - T_{0g}) = 36.5$ and $\tau_0 = 3.14 \times 10^{-15}$ s with $B/(T_g - T_{0g}) = 38$ in all glasses [3,9,27]. Equation (17) giving τ_0 is used to determine $\ln A_g$ only, depending on $\{\ln(1 + \theta_{2lgs}) - \ln[V_m \times \Delta S_m]\}$.

With $\tau_0 = 1.4 \times 10^{-14}$ s, the $\ln A_g$ is equal to 100.7 in N 6 Pd₄₃Ni₁₀Cu₂₇P₂₀ ($V_m = 8 \times 10^{-6}$ m³, $\Delta S_m = 8.74$ J/K, $\theta_{2lgs} = -0.271$) and to 96.4 in N 20 Glycerol ($V_m = 73.07 \times 10^{-6}$ m³, $\Delta S_m = 62.42$ J/K, $\theta_{2lgs} = -0.352$).

With $\tau_0 = 3.14 \times 10^{-15}$ s, the $\ln A_g$ is respectively equal to 102.2 and 97.9 for the same liquids with an increase of the product $V_m \times \Delta S_m$ by a factor 66.

With $\tau_0 = 1.4 \times 10^{-14}$ s, the average value of $\ln A_g$ is 98.5 ± 2 and with $\tau_0 = 3.14 \times 10^{-15}$ s, $\ln A_g = 100 \pm 2$. The $\ln K_{lgs}$ and the thermally-activated energy barrier $\Delta G^*_{2lgs}/k_B T_g$ are always equal to 62 ± 2 in all glass-forming melts at $T = T_g$.

Equation (15) shows that the assumption of a value of τ_0 being the same in all melts can be replaced by a nearly-constant value of A_g ; $\ln A_g$ is about 15% larger than the one found for crystal nucleation from surviving crystals in several glass-forming melts at higher temperatures [14]. Then, the time lag of a transient nucleation to produce a crystal nuclei distribution, built from surviving crystals and ready for steady-state nucleation, is about 10^6 times larger than the time lag τ_g^{ns} required for a homogeneously-nucleated cluster distribution formation. The steady-state nucleation time t_{sn} is, in addition, equal to 10^9 s for $v = 10^{-9}$ m³. A nucleus distribution with cluster size close to the critical value is created just near T_g when the relaxation time is minimum. In Turnbull and Fisher's model, $\ln K_{ls}$ is nearly equal to $\ln(N_A k_B T^*_g / V_m h) - \Delta f^*/k_B T^*_g$ where h is Planck's constant and $\Delta f^*/k_B T^*_g$ is a thermally-activated energy barrier for atom diffusion from the melt to the homogeneously-nucleated cluster which is smaller than the one from the melt to a surviving crystal [65]. This weakening could be due to formation of clusters containing many vacancies on their various sub-lattices during homogeneous nucleation. Surviving crystals are expected to be well-crystallized because they are part of previously-crystallized materials. They did not melt above T_m and they are very stable with their fusion heat equal to the bulk one [21-23].

3.3. The Thermodynamic Vitreous Transition T^*_g at the Disappearance Temperature of the Fully-Relaxed Enthalpy

A relaxed enthalpy is measured by DSC, after quenching the undercooled liquid to much lower temperatures than T_g and annealing it at a temperature T_a smaller than T_g , during the relaxation time necessary to obtain its maximum value H_r . The structural relaxation is viewed as a transformation of

the quenched undercooled liquid state in a fully-frozen state. This exothermic heat varies linearly with $(T_g^* - T_a)$ as shown in Figures 2 and 3. The fully-relaxed enthalpies H_r of As_2Se_3 and $\text{Zr}_{58.5}\text{Cu}_{15.6}\text{Ni}_{12.8}\text{Al}_{10.3}\text{Nb}_{2.8}$ (vit106a) are plotted in Figure 2 using values of T_g^* equal to 462 and 690 K instead of $T_g = 450$ and 673 K respectively [54,66,67]. The calculated temperatures T_{0g} are respectively 293 K and 437 K as compared to $T_{02} = 335$ and 437 K. The vitreous transition T_g^* of As_2Se_3 exactly corresponds to the mid-point of the reversible specific heat jump [67]. In Figure 3 we describe the relaxed enthalpy variation of propylene glycol and glycerol extracted from two different publications with $T_g^* = 171$ and 189.8 K instead of $T_g = 167$ and 190 K respectively [68,69]. The calculated temperatures T_{0g} are respectively 112 K and 121 K as compared to $T_{02} = 117$ and 128 K.

The specific heat excess of the undercooled melt ΔC_{pgl} can be directly calculated from $dH_r/dT_a = \Delta C_{pgl}$ because H_r is a linear function of T_a and $H_r = \int_{T_a}^{T_g^*} \Delta C_{pgl} dT$. The following calculated values of ΔC_{pgl} are in good agreement with the specific heat difference ΔC_{pls} between solid and liquid; for propylene glycol, $\Delta C_{pgl} = 52.3$ and $\Delta C_{pls} = 67.3$ J/mole/K [68,69]; for glycerol, $\Delta C_{pgl} = 69.9$ and $\Delta C_{pls} \cong 79.4$ J/mole/K [32,68,69]; for vit106a, $\Delta C_{pgl} = 13.5$ and $\Delta C_{pls} \cong 15.5$ J/mole/K [54]; for As_2Se_3 , $\Delta C_{pgl} = 67$ J/mole/K from the relaxed enthalpy and 67 J/mole/K from the reversible specific heat [67]. The specific heat jump ΔC_{pls} is a little too large at T_g when it is measured at a too low heating rate because it still contains an endothermic contribution except when stepscan techniques are used [13].

Figure 2. The saturated value of the relaxed enthalpy H_r is plotted *versus* $(T_g^* - T_a)$, T_g^* being the thermodynamic vitreous transition and T_a the annealing temperature; for N°35 vit 106a ($\text{Zr}_{58.5}\text{Cu}_{15.6}\text{Ni}_{12.8}\text{Al}_{10.3}\text{Nb}_{2.8}$), $T_g^* = 690$ K and the slope of the straight line $\Delta C_{pgl} = 13.5$ J/g.atom and for N° 10 As_2Se_3 , $T_g^* = 462$ K and $\Delta C_{pgl} = 13.5$ J/g.atom [54,66,67]. The corresponding values of T_{0g} calculated from T_g^* are 443 K and 293 K. The deviation from the straight line is due to the approach of the Kauzmann temperature of As_2Se_3 [67].

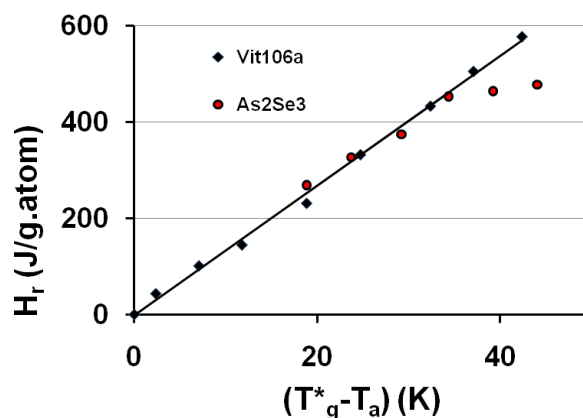
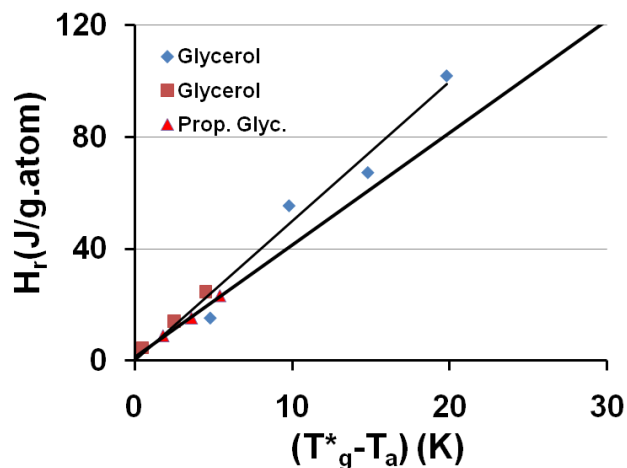


Figure 3. The saturated value of the relaxed enthalpy H_r is plotted *versus* $(T_g^* - T_a)$, T_g^* being the thermodynamic vitreous transition and T_a the annealing temperature; for N ° 20 glycerol, $T_g^* = 189.8$ K and the slope of the straight line $\Delta C_{pgl} = 4.99$ J/g.atom and for N ° 2 propylene glycol $T_g^* = 171$ K and $\Delta C_{pgl} = 4.02$ J/g.atom. The corresponding values of T_{0g} calculated from T_g^* are 121 and 112 K respectively. The largest values of H_r are due to [68] and the smallest ones to [69].



The specific heat excess of an undercooled melt tends to zero at the Kauzmann temperature as shown by the fact that the derivative $d\Delta H_r/dT$ of As_2Se_3 tends to zero at this temperature as reproduced in Figure 2 [66,67]; the Kauzmann temperature T_k is an actual temperature of undercooled melts instead of a virtual one [67].

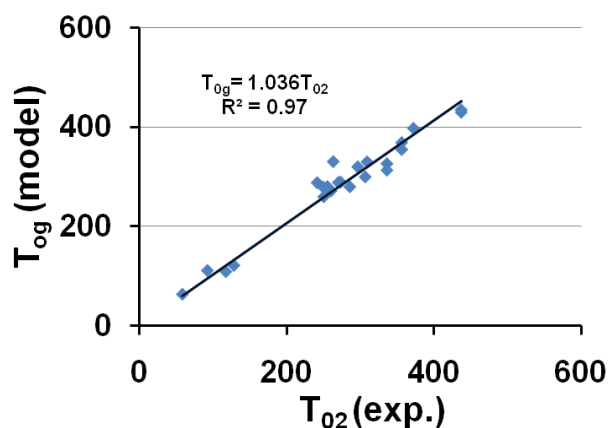
3.4. The Crystal Homogeneous Nucleation Temperature at T_g^*

The vitreous transition T_g^* (or θ_g^*) is viewed as occurring at the crystal steady-state nucleation maximum-rate temperature T_{2lgs} (or θ_{2lgs}). In this case, the glass transition being a material constant has to obey (6). The energy saving approximate coefficients ε_{lgs0} in Table 1 are given by (18) using T_g which is not known instead of T_g^* :

$$\varepsilon_{lgs0} = 1.5 \times \theta_g + 2 \quad (18)$$

The corresponding temperatures $T_{0g} = T_{0lgs}$ (or $\theta_{0g} = \theta_{0lgs}$) listed in Table 1, are calculated from ε_{lgs0} determined by (18) and (7,8). The calculated temperature T_{0g} of the free volume disappearance is plotted as a function of the VFT temperature T_{02} in Figure 4. The average of T_{0g} is 3.6% larger than that of T_{02} . These quantities are nearly equal if we consider that T_g is an out-of-equilibrium temperature which is not exactly equal to the thermodynamic transition T_g^* . The model works and is able to predict the VFT temperature of fragile glass-forming melts when T_g^* is known.

Figure 4. The calculated values of the free-volume disappearance temperature T_{0g} of fragile glass-forming melts are plotted *versus* the VFT temperatures T_{02} determined by measurements in the vicinity of T_g ; $T_{0g} \cong 1.036 T_{02}$.



The energy saving coefficients ϵ_{lg0} and ϵ_{ls0} are not equal and correspond to the two reduced temperatures θ_{0g} and θ_{0m} given by (6). The coefficient ϵ_{ls0} is calculated using T_{0m} and T_g of N° 29 vit105 ($Zr_{52.5}Cu_{17.9}Ni_{14.6}Al_{10}Ti_5$) because the scaling law $T_{0m} = 0.77 \times T_g$ [7,64] is obeyed by this material. $\Delta\epsilon(\theta_g) = (\epsilon_{ls0} - \epsilon_{lg0})$ is equal to 0 for $\theta_g = 0$ and 0.19 for $\theta_g = -0.381$. These two particular values are used to determine a possible scaling law followed by $\Delta\epsilon$. The crystal nucleation maximum-rate temperature θ_{2ls} is given by (7,8) as a function of ϵ_{ls0} ; then, ϵ_{ls0} and $\epsilon_{ls0} - \epsilon_{lg0} = \Delta\epsilon$ have to be linear functions of θ_g given by (11):

$$\epsilon_{ls0} = \theta_g + 2 \tag{19}$$

$$\epsilon_{ls0} - \epsilon_{lg0} = \Delta\epsilon = -0.5 \times \theta_g \tag{20}$$

The two energy saving coefficients ϵ_{ls0} and ϵ_{lg0} given in Table 1 are plotted as a function of θ_g in Figure 5. Equations (7) and (8) are used to predict the temperatures T_{0g} and T_{0m} also given in Table 1 and plotted as a function of T_g in Figure 6. These values are the free-volume disappearance temperatures of glass-forming melts having a thermodynamic glass transition occurring at $T_g^* = T_g$.

Figure 5. The energy saving coefficients ϵ_{ls0} and ϵ_{lg0} are calculated respectively using the scaling laws (18) and (19,20) and are plotted *versus* $\theta_g = (T_g - T_m)/T_m$.

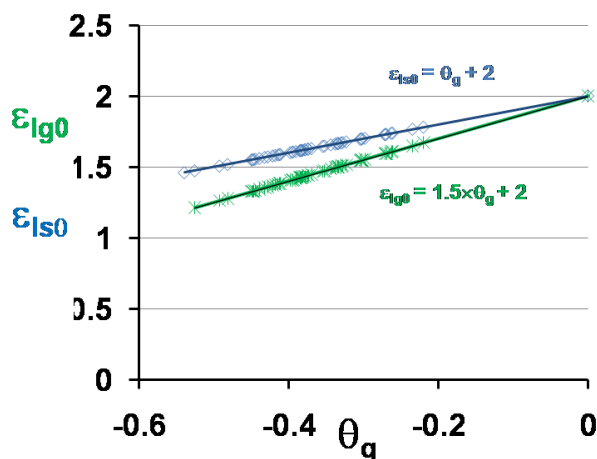
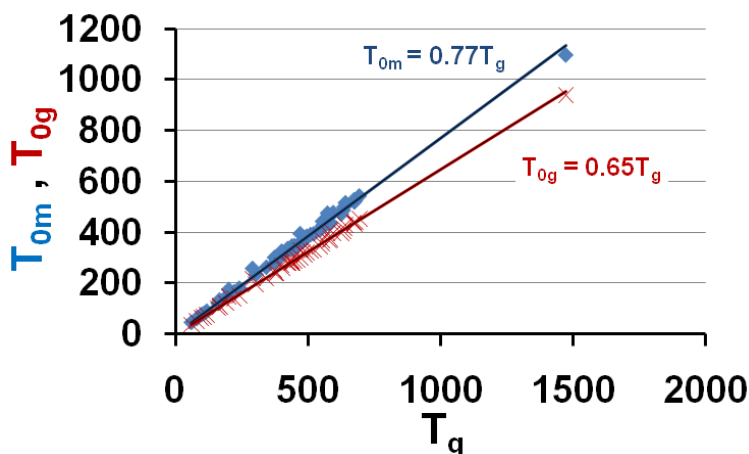


Figure 6. The calculated values of the free-volume disappearance temperatures T_{0m} and T_{0g} are plotted *versus* T_g ; they are equal to the VFT temperatures T_{01} and T_{02} represented in Figure 1. $T_{0m} = 0.77 T_g$ and $T_{0g} = 0.65 T_g$.



These predictions are in very good agreement with experiments when we compare Figure 6 to Figures 1 and 4. Then, the vitreous transition corresponds to a crystal homogeneous nucleation temperature. A distribution of homogeneously-nucleated clusters is created when the temperature decreases down to T_g^* . The scaling laws (18) and (19) are obeyed and reflect intrinsic properties of glass-forming melts. The two VFT temperatures corresponding to two free-volume disappearance temperatures follow intrinsic scaling laws related to a change of the energy saving in all melts. These predictions can be more precise as shown in Figures 7 and 8. In fact, the ratios T_{0m}/T_g and T_{0g}/T_g are weakly varying with the glass transition; the proportionality coefficients 0.77 and 0.65 are mean values for a lot of glasses and polymers having θ_g values larger than -0.45 and smaller than -0.2 . The ratio T_{0m}/T_{0g} is nearly constant in the same interval of θ_g values as shown in Figure 6; it tends to 1 when θ_g tends to 0 and $-2/3$.

Figure 7. The ratios T_{0g}/T_g and T_{0m}/T_g of the free-volume disappearance temperatures to the glass transition temperature T_g are plotted *versus* $\theta_g = (T_g - T_m)/T_m$.

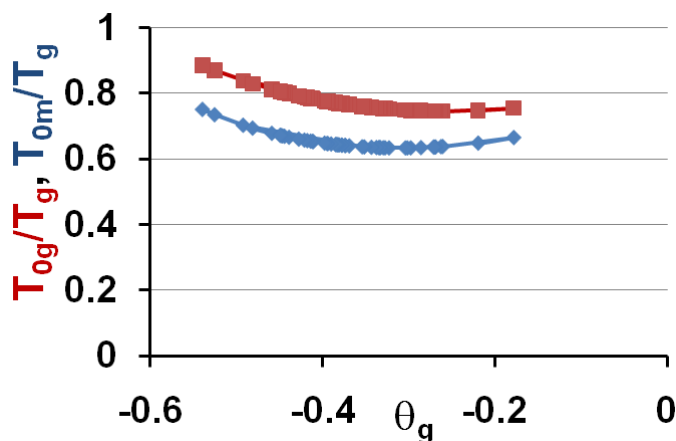
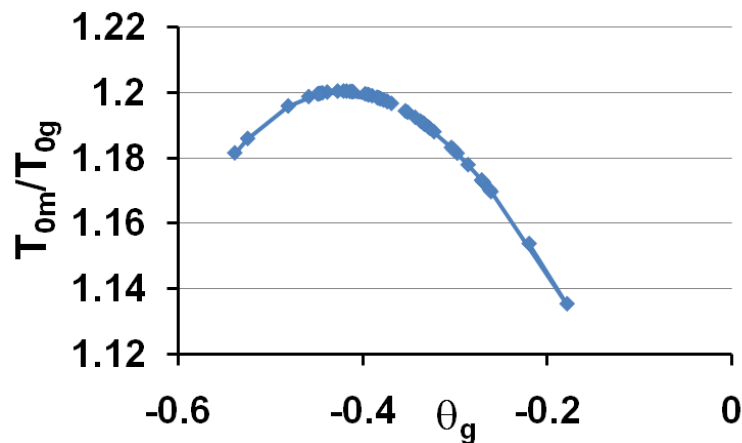


Figure 8. The ratios of the free-volume disappearance temperatures T_{om}/T_{og} are plotted versus $\theta_g = (T_g - T_m)/T_m$.



3.5. Volume Energy Saving Associated with Nascent Crystals in Non-Metallic Glass-Forming Melts

Volume energy saving associated with homogeneously-nucleated crystal formation also exists in non-metallic liquids. It could be due to an electrostatic interaction between a screen of ionic charges present in the melt and charges carried by homogeneously-nucleated crystals containing unoccupied ionic sites. Homogeneous nucleation gives rise, in a first step, to ultra-fine crystals among density fluctuations. Ions of opposite charges could be randomly distributed inside their own sub-lattices in a crystal. The mean charge carried by such crystals would be proportional to the square root of their atom number n . Counter-ions of opposite charge would screen the grain charge and induce an attractive interaction proportional to the square of the grain charge and then to the atom number n . Neel already made a similar assumption to explain the superparamagnetic (ferrimagnetic) properties of antiferromagnetic ultra-fine grains. The superparamagnetic Curie constant of ultra-fine grains is equal to the Curie constant of n paramagnetic atoms because the magnetic moments carried by different ions are randomly distributed in their own sub-lattices and the grain uncompensated magnetic moment is proportional to $n^{1/2}$ [70].

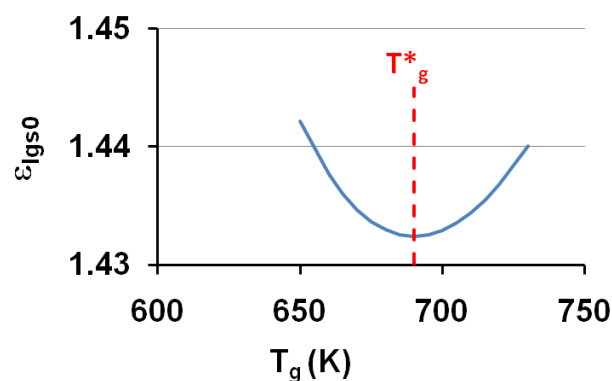
The presence of volume energy saving in nonmetallic glass-forming melts is also due to a more general phenomenon associated with the formation of noncritical clusters in melts containing n atoms. The chemical potential of a small cluster is expected to differ from the bulk value. A new contribution $-(p - p_0)V_m$ ought to be added to the classical Gibbs free energy change. It depends on the Laplace pressure p applied to the cluster when a cluster is formed, p_0 being the classical pressure of the melt on the solid particle, regardless of its size. This complementary contribution is not involved in the classical Gibbs free energy change because the pressure p is not homogeneous in the melt [71]. The Laplace pressure p increases with a decreasing atom number n . In addition, the energy saving is quantified when the critical cluster radius and the number of transferred electrons are very small in metallic glass-forming melts [14-15]. The temperature dependence of ε_{ls} given by (1) is a general law for nascent clusters in all melts.

3.6. Thermodynamic Origin of Relaxed Enthalpy and of Out-of-Equilibrium Nucleation Temperatures T_g

Enthalpy is relaxed at the annealing temperature $T_a < T_g^*$ applied after quenching the undercooled melt down to a much lower temperature. The fully-relaxed enthalpy is equal to $H_r = \Delta C_{plg}(T_g^*) \times [T_g^* - T_a]$ for $T_k < T_a < T_g^*$ instead of being related to the enthalpy excess stored by an undercooled melt quenched from T_a down to the Kauzmann temperature T_k and to the entropy available below T_a . So this relaxed enthalpy correlated to the thermodynamic transition.

The annealing temperature T_a is an out-of-equilibrium homogeneous nucleation temperature of a fragile glass-forming melt and a solution of (6) corresponding, for the same value of θ_{0lg} , to an energy saving coefficient of nascent crystals at T_m being a little larger than the equilibrium value at a nucleation temperature equal to T_g^* [15]. The annealing temperature T_a is a temporary nucleation temperature during the time lag of the transient nucleation. The undercooled melt progressively relaxes enthalpy and entropy excesses stored between T_a and T_g^* towards their equilibrium values at T_g^* . The existence of this relaxed enthalpy is a strong argument in favor of a thermodynamic equilibrium at T_g^* . The time-dependent vitreous transition T_g is due to this endothermic heat appearing at a temperature varying with the heating rate in a DSC run. A nucleation temperature $T_{2ls} = T_g$ could also exist above T_g^* when high heating rates are used because the homogeneous nucleation temperature T_{2ls} only depends on the energy saving coefficient ε_{lgso} for a well-defined ideal glass transition temperature T_{0g} (or θ_{0g}) as shown by (6) and Figure 9.

Figure 9. The out-of-equilibrium homogeneous nucleation temperatures $T_{2ls} = T_g$ equal to homogeneous nucleation temperatures depend on energy saving coefficients ε_{lgso} through (6). The equilibrium transition of vit 106a ($Zr_{58.5}Cu_{15.6}Ni_{12.8}Al_{10.3}Nb_{2.8}$) at $T_g^* = 690$ K has been previously determined as shown in Figure 2. The temperature $T_{0g} = 437$ K is equal to T_{02} .



A spin-glass transition is also characterized in zero field by the presence at once of a time-dependent susceptibility cusp temperature, a phase transition temperature and, in the magnetic field, by two lines of transition $H_c(T)$ and $H_m(T)$ [72]. The phase diagram (H,T) of Cu–Mn has been investigated by measuring magnetocaloric effects showing the importance of the entropy $S(T,H)$ in understanding the physics of spin glass transition. The $H_c(T)$ is the boundary line spin-glass/non-Curie paramagnet. The $H_m(T)$ is a cross-over line Curie/Non-Curie paramagnet corresponding to an irreversibility line and to a freezing of rigid clusters of spins [72-74]. The spin-glass phase transition

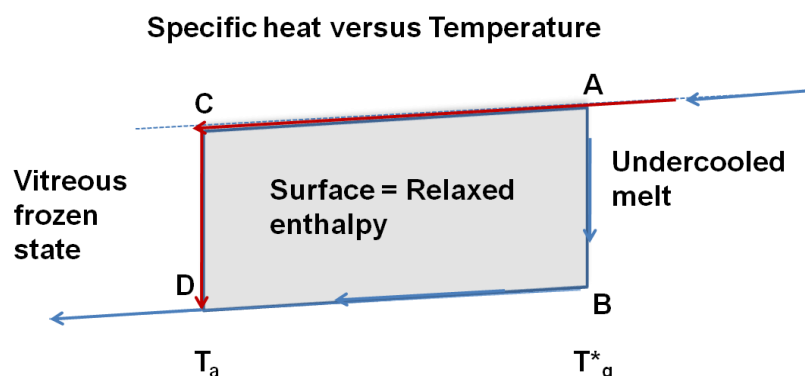
can be separated from the irreversibility line when the magnetic field frequency increases. The existence of this type of phenomenon in glasses remains an open question because the reversible specific heat jump always occurs in As_2Se_3 at the same vitreous transition regardless of the heating and cooling rates [67].

4. Summary and Complementary Information on the Two Crystal Nucleation Temperatures

New equations governing the crystal nucleation, reflecting the energy saving associated with Fermi energies equalization of nascent crystals and melt, have been used and applied to all glass-forming melts. The vitreous transition is characterized by freezing at a crystal homogeneous nucleation temperature only determined by thermodynamics considerations. We have shown, for the first time, that an energy scale governs the vitreous transition. This material constant does not strictly depend on the viscosity, even if the viscosity is high and nearly the same at T_g^* , because the energy barrier for crystal growth nucleation ΔG_{2ls}^* divided by $k_B T_g$ is nearly the same in all glass-forming melts. The energy barrier Δf^* to transfer an atom from the melt to a nascent crystal divided by $k_B T_g^*$ is also nearly the same and is a little smaller than the one from transport across the melt-crystal interfaces at the first crystallization temperature which is induced by surviving intrinsic crystals.

These findings are in agreement with published works having shown that the reversible specific heat jump at T_g^* does not depend on time and on sample thermal history. In addition, the relaxed enthalpy disappears at the thermodynamic transition T_g^* and its maximum value obtained at each annealing temperature T_a after quenching the undercooled liquid to lower temperatures, is given by $H_r = \int_{T_a}^{T_g^*} \Delta C_{pgl} dT$, ΔC_{pgl} being the specific heat jump at T_g^* . The apparent specific heat jump at T_g calculated from the heat flux measurement is equal to the reversible one. The specific heat jump deduced from heat flux measurement occurs at a temperature T_g depending on the heating rate. There is no visible anomaly at T_g^* in a DSC run. This phenomenon is schematized in Figure 10. The glass transition temperatures T_g determined by DSC correspond to out-of-equilibrium crystal homogeneous nucleation temperatures and to out-of-equilibrium values of the energy saving coefficient ϵ_{lg0} .

Figure 10. The reversible thermodynamic vitreous transition occurs at $T = T_g^*$; the specific heat decreases along AB; the specific heat of the vitreous fully-frozen state along BD is equal to the crystallized state. The undercooled melt is quenched at low temperatures and annealed at the temperature T_a . The transformation from C to D relaxes an enthalpy equal to the surface ABDC when the time-lag necessary for cluster formation has evolved.



The thermodynamic transition T_g^* is a linear function of the energy saving divided by the fusion heat associated, in a nascent crystal formation, with the equalization of Fermi energy or chemical potential of nascent crystals and glass-forming melts. It is possible to predict, only using T_g^* and the melting temperature T_m , a free-volume disappearance temperature equal to the VFT temperature of fragile-glass-forming melts deduced from viscosity and relaxation time measurements above and near T_g^* . There are two crystal homogeneous nucleation temperatures which follow scaling laws linearly dependent on two energy saving coefficients ε_{s0} in the crystal formation as there are two VFT temperatures.

Experimentally, the first-crystallization temperature occurs when cooling the glass-forming melt at a lesser rate than the critical one, down to a temperature that is higher than the homogeneous nucleation temperature and is generally induced by intrinsic heterogeneous crystals which reduce the energy barrier for crystal growth. The isothermal crystallization time depends on overheating and undercooling temperatures and leads to a time-temperature-transformation diagram induced by intrinsic nuclei. The nose temperature of this diagram depends on the overheating temperature, the surviving crystal size and the energy saving ε_s .

The second nucleation temperature is lower and gives rise by homogeneous nucleation to imperfect crystals having an energy barrier for diffusion from the melt to the crystal slightly smaller than the first. The free-volume disappearance temperature of the undercooled melt decreases from T_{0m} to T_{0g} . A glass state is obtained by quenching the melt using a cooling rate larger than its critical value. The vitreous transition temperature T_g^* occurs at a homogeneous nucleation maximum-rate temperature determined by a smaller value $\varepsilon_{lgs}(\theta_g)$ of the energy saving associated with a smaller VFT temperature. The relaxation time leading to vitreous state is the time lag for initial formation of a homogeneously-nucleated-cluster distribution during the transient nucleation. These entities could be imperfect crystals. Their formation is a preliminary step during the long time leading to crystallization. The time dependence of various properties depends on the time lag τ^{ns} associated to the transient nucleation and to the steady-state nucleation time t_{sn} depending on the energy barrier for crystal growth.

The model used in this paper is also based on previous publications related to the classical Gibbs free energy change for a crystal formation in an undercooled melt that has been completed by an energy saving associated with the equalization of Fermi energies or chemical potentials of melt and nascent crystal. This analysis only works for nascent crystals in an out-of-equilibrium state having a radius smaller than the critical radius for crystal growth because J. W. Gibbs's phase coexistence rule predicts the absence of energy saving for radii larger than the critical one when solid and liquid phases are at equilibrium at the melting temperature.

5. Conclusions

The vitreous transition is a new type of phase transition from undercooled melt to frozen state, without entropy and enthalpy change occurring at a temperature T_g^* , which corresponds to the maximum nucleation rate temperature of homogeneously-nucleated crystals in bulk metallic and non-metallic glass-forming melts. Because of the melt freezing, the steady-state nucleation time is too

long to ever reach the divergence of the correlation length in critical phenomenon and the crystal's growth.

These nascent crystals would be formed with a free energy change which differs from the classical Gibbs free energy change used in many nucleation models. A complementary energy saving exists which depends on the atom or molecule number n involved in these crystals. We have shown the existence of two homogeneous nucleation temperatures associated with two energy savings, which follow scaling laws as a function of the vitreous transition temperature. The nascent crystals acting at the vitreous transition could contain a lot of unoccupied ionic sites as compared with crystals surviving in the melt and acting as growth nuclei at higher temperatures.

The glass freezing occurs without entropy and enthalpy changes; these changes can only appear at unattainable times when crystallization occurs. This analysis shows that the frozen and the solid states have the same equilibrium specific heat below the glass transition, eliminating all speculations about other configurational contributions and phase transitions.

The disappearance temperature of the fully-relaxed enthalpy, as described in previous publications, does not depend on time and is equal to the thermodynamic temperature T^*_g . The specific heat jump accompanying this phase transition is deduced from the linear variation of the relaxed enthalpy with temperature. The DSC runs are not able to detect T^*_g because the enthalpy is continuous at this temperature.

The existence of a vitreous transition viewed as a constant of material was initially established by experiments eight years ago and published by the University of Pardubice.

Acknowledgements

This work was also sponsored by the sino-french Laboratory for the Application of Superconductors and Magnetic Materials involving the Northwest Institute for Non-ferrous Metal Research (NIN), the Northwestern Polytechnical University (NPU) in Xi'an (P.R. China). Thanks are due to Lian Zhou for NIN support as, Jean Etourneau, Philippe Odier, Jean-Louis Soubeyroux, Jean-Louis Tholence for their suggestions or their criticisms, Dr Jinna Mei from NPU and J.L. Soubeyroux for fully-relaxed enthalpy measurements of some glass-forming melts [75].

References

1. Zarzycki, J. *Les Verres et l'Etat Vitreux*; Masson: Paris, France, 1982.
2. Gutzov, I.; Schmelzter, J. *The Vitreous State*; Springer-Verlag: Berlin, Germany, 1995.
3. Angell, C.A. Formation of glasses from liquids and biopolymers. *Science* **1995**, *267*, 1924-1935.
4. Berthier, L.; Biroli, G.; Bouchaud, J.; Cipelletti, L.; Masri, D.E.; L'Hôte, D.; Ladieu, F.; Pierno, M. Direct experimental evidence of a growing length scale accompanying the glass transition. *Science* **2005**, *310*, 1797-1800.
5. Tanaka, H.; Awasaki, T.; Shintani, H.; Watanabe, K. Critical-like behavior of glass-forming liquids. *Nature Mater.* **2010**, *9*, 324-331.
6. Kauzmann, W. The nature of the glassy state and the behavior of liquids at low temperatures. *Chem. Rev.* **1948**, *43*, 219-256.

7. Liu, C.-Y.; He, J.; Keunings, R.; Bailly, C. New linearized relation for the universal viscosity-temperature behavior of polymer melts. *Macromolecules* **2006**, *39*, 8867-8869.
8. Williams, M.L.; Landel, R.F.; Ferry, J.D. Temperature dependence of relaxation mechanisms in amorphous polymers and other glass-forming melts. *J. Am. Chem. Soc.* **1955**, *77*, 3701-3707.
9. Takeuchi, A.; Kato, H.; Inoue, A. Vogel-Fulcher-Tammann plot for viscosity scaled with temperature interval between actual and ideal glass transitions for metallic glasses in liquid and supercooled liquid states. *Intermetallics* **2010**, *18*, 406-411.
10. Doolittle, A.K. Studies in Newtonian Flow. II. The dependence of the viscosity of liquids on free-space. *J. Appl. Phys.* **1951**, *22*, 1471-1475.
11. Ramachandrarao, P.; Dubey, K.S. A thermodynamic approach to the viscous behaviour of glass-forming liquids. *Mat. Sc. Eng. B* **1995**, *32*, 285-293.
12. Gibbs, J.H.; DiMarzio, E.A. Nature of the glass transition and the glassy state. *J. Chem. Phys.* **1958**, *28*, 373-383.
13. Holubov à J.; Cernozek, Z.; Cernoskov à E. The study of the glass transition by the stepscan DSC technique. *J. Optoelectron. Adv. Mat.* **2005**, *7*, 2671-2676.
14. Tournier, R.F. Crystal growth nucleation and Fermi energy equalization of intrinsic spherical nuclei in glass-forming melts. *Sci. Technol. Adv. Mater.* **2009**, *10*, 014607:1-014607:12.
15. Tournier, R.F. Crystal nucleation and equalization of Fermi energies of intrinsic nuclei and glass-forming melts. *J. Phys. Confer. Ser.* **2009**, *144*, 012116:1-012116:4.
16. Tournier, R.F. Presence of intrinsic growth nuclei in overheated and undercooled liquid elements. *Phys. B* **2007**, *392*, 79-93.
17. Vinet, B.; Magnusson, L.; Fredriksson, H.; Desr é P.J. Correlations between surface and interface energies with respect to crystal nucleation. *J. Coll. Interf. Sci.* **2002**, *255*, 363-374.
18. Turnbull, D.; Cech, R.E. Microscopic observation of the solidification of small metal droplets. *J. Appl. Phys.* **1950**, *21*, 804-810.
19. Bosio, L.; Defrain, A.; Epelboin, I. Changements de phase du gallium à la pression atmosphérique. *J. Phys. France* **1966**, *27*, 61-71.
20. Hays, C.C.; Johnson, W.L. Undercooling of bulk metallic glasses processed by electrostatic levitation. *J. Non-Cryst. Solids* **1999**, *250-252*, 596-600.
21. Tournier, R.F. Expected properties of gold melt containing intrinsic nuclei. In *Proceedings of the 6th International Conference on Electromagnetic Processing of Materials, EPM 2009*, Dresden, Germany, 19–23 October 2009; pp. 304-307.
22. Tournier, R.F. Undercooling versus Overheating of Liquid Elements Containing Intrinsic Nuclei: Application to Magnetic Texturing. Presented at *the 4th International Workshop on Materials Analysis and Processing in Magnetic Fields Organized by Hamid Garmestani*, Atlanta, GA, USA, 10–12 May 2010.
23. Tournier, R.F. Nucleation of crystallization in titanium and vitreous state in glass-forming melt. In *Proceedings of the 12th World Conference on Titanium*, Beijing, China, 19–24 June 2011.
24. Hirata, A.; Hirotsu, Y.; Ohkubo, T.; Hanada, T.; Bengus, V.Z. Compositional dependence of local atomic structures in amorphous Fe_{100-x}B_x alloys studied by electron diffraction and high-resolution electron microscopy. *Phys. Rev. B* **2006**, *74*, 214206:1-214206:9.

25. Sidorov, V.; Popel, P.; Calvo-Dahlborg, M.; Dahlborg, U.; Manov, V. Heat treatment of iron-based melts before quenching. *Mater. Sc. Eng. A* **2001**, *304-306*, 480-486.
26. Kokshenev, V.B. Characteristic temperatures of liquid-glass transition. *Phys. A* **1999**, *262*, 88-97.
27. Busch, R.; Liu, W.; Johnson, W.L. Thermodynamics and kinetics of the Mg₆₅Cu₂₅Y₁₀ bulk metallic glass forming liquid. *J. Appl. Phys.* **1998**, *83*, 4134-4441.
28. Shadovskaya, L.; Busch, R. On the fragility of Nb-Ni-based and Zr-based bulk metallic glasses. *Appl. Phys. Lett.* **2004**, *85*, 2508-2510.
29. Lu, I.-R.; Görlner, G.P.; Willnecker, R. Specific volume of glass-forming liquid Pd₄₃Cu₂₇Ni₁₀P₂₀ and related thermodynamic aspects of the glass transition. *Appl. Phys. Lett.* **2002**, *80*, 4534-4536.
30. Yavari, A.R.; Le Moulec, A.; Nishiyama, N.; Inoue, A.; Vaughan G.; Kvick, A.; Botta, W.J. Glass Transition T_g and quenched-in free volume in bulk metallic glasses measured by X-ray diffraction. *J. Metast. Nanocryst. Mater.* **2004**, *20-21*, 23-28.
31. Nishiyama, N.; Inoue, A. Glass transition behavior and viscous flow working of Pd₄₀Cu₃₀Ni₁₀P₂₀ amorphous alloy. *Mater. Trans. JIM* **1999**, *40*, 64-71.
32. Dubey, K.S.; Ramachandrarao, P.; Lele, S. Thermodynamic and viscous behavior of undercooled liquids. *Thermochim. Acta* **1996**, *280/281*, 25-62.
33. Kouamé N.; Sei, J.; Houphouët-Boigny, D.; Kra, G.; Jumas, J.C.; Olivier-Fourcade, J. Propriétés thermiques et optiques des verres du système Sb₂S₃-As₂S₃. *C. R. Chimie* **2007**, *10*, 498-501.
34. Birge, N.O. Specific heat spectroscopy of glycerol and propylene glycol near the glass transition. *Phys. Rev. B* **1986**, *34*, 1631-1642.
35. Schönhals, A.; Kremer, F.; Hofmann, A.; Fischer, E.W. Anomalies in the scaling of the α -relaxation studied by dielectric spectroscopy. *Phys. A* **1993**, *201*, 263-269.
36. Mishra, R.K.; Dubey, K.S. Glass-forming ability of materials: A thermodynamic approach. *J. Non-Cryst. Sol.* **2009**, *355*, 2199-2204.
37. Yang, Z.; Lam, C.H.; Dimasi, E.; Bouet, N.; Jordan-Sweet, J.; Tsui, O.K.C. Method to measure the viscosity of nanometer liquid films from the surface fluctuations. *Appl. Phys. Lett.* **2009**, *94*, 251906:1-251906:3.
38. Lu, I.-R.; Wilde, G.; Görlner, G.P.; Willnecker, R. Thermodynamic properties of Pd-based glass-forming alloys. *J. Non-Cryst. Sol.* **1999**, *250-252*, 577-581.
39. Schroers, J. On the formability of bulk metallic glass in its supercooled liquid state. *Acta Mater.* **2008**, *56*, 471-478.
40. Johari, G.P. Heat capacity and entropy of an equilibrium liquid from T_g to 0 K, and examining the conjectures of an underlying thermodynamic transition. *Chem. Phys.* **2001**, *265*, 217-231.
41. Henderson, D.W.; Ast, D.G. Viscosity and crystallization kinetics of As₂Se₃. *J. Non-Cryst. Sol.* **1984**, *64*, 43-70.
42. Waniuk, T.A.; Busch, R.; Masuhr, A.; Johnson, W.L. Equilibrium viscosity of the Zr_{41.2}Ti_{13.8}Cu_{12.5}Ni₁₀Be_{22.5} bulk metallic glass-forming liquid and viscous flow during relaxation, phase separation, and primary crystallization. *Acta Mater.* **1998**, *46*, 5229-5236.
43. Lu, Z.P.; Li, Y.; Liu, C.T. Glass-forming tendency of bulk La-Al-Ni-Cu-(Co) metallic glass-forming melts. *J. Appl. Phys.* **2003**, *93*, 286-290.
44. Lu, Z.P.; Liu, C.T. A new glass-forming ability criterion for bulk metallic glasses. *Acta Mater.* **2002**, *50*, 3501-3512.

45. Lu, Z.P.; Li, Y.; Ng, S.C. Reduced glass transition temperature and glass forming ability of bulk glass forming alloys. *J. Non-Cryst. Sol.* **2000**, *270*, 103-114.
46. Angell, C.A.; Rao, K.J. Configurational excitations in condensed matter, and the “bond lattice” model for liquid-glass transition. *J. Chem. Phys.* **1971**, *57*, 470-481.
47. Hatase, M.; Hanaya, M.P.; Hikima, T.; Oguni, M. Discovery of homogeneous-nucleation-based crystallization in simple glass-forming liquid of toluene below its glass-transition temperature. *J. Non-Cryst. Sol.* **2003**, *307-310*, 257-263.
48. Kato, H.; Wada, T.; Hasegawa, M.; Saida, J.; Inoue, A. Fragility and thermal stability of Pt- and Pd-based bulk glass forming liquids and their correlation with deformability. *Scripta Materialia* **2006**, *54*, 2023-2027.
49. Kui, H.-W.; Turnbull, D. The heat capacity of Ni₄₀Pd₄₀P₂₀ in the liquid, glass and crystallized states. *J. Non-Cryst. Sol.* **1987**, *94*, 62-69.
50. Legg, B.A.; Schroers, J.; Busch, R. Thermodynamics, kinetics, and crystallization of Pt_{57.3} Cu_{14.6} Ni_{5.3} P_{22.8} bulk metallic glass. *Acta Mater.* **2007**, *55*, 1109-1116.
51. Chen, H.S.; Goldstein, M. Anomalous visco-elastic behavior of metallic-glasses of Pd–Si-based alloys. *J. Appl. Phys.* **1972**, *43*, 1642-1648.
52. Mukherjee, S.; Schroers, J.U.; Zhou, Z.; Johnson W.L.; Rhim, W.-K. Viscosity and specific volume of bulk metallic glass-forming alloys and their correlation with glass-forming stability. *Acta Mater.* **2004**, *52*, 3689-3695.
53. Mälek, J.; Svoboda, R.; Pustkova, P.; Cicmanec, P. Volume and enthalpy relaxation of a-Se in the glass transition region. *J. Non-Cryst. Sol.* **2009**, *355*, 264-272.
54. Gallino, I.; Shah, M.B.; Busch, R. Enthalpy relaxation and its relation to the thermodynamics and crystallization of the Zr_{58.5}Cu_{15.6}Ni_{12.8}Al_{10.3}Nb_{2.8} bulk metallic glass-forming alloy. *Acta Mater.* **2007**, *55*, 1367-1376.
55. Meng, Q.G.; Zhang, S.G.; Li, J.G.; Bian, X.F. Strong liquid behavior of Pr₅₅Ni₂₅Al₂₀ bulk metallic glass. *J. Alloys Compounds* **2007**, *431*, 191-196.
56. Huang, H.J.; Shen, J.; Sun, X.B.; Yu, J.F. A new Ti–Zr–Hf–Cu–Ni–Si–Sn bulk amorphous alloy with high glass-forming ability. *J. Alloys Compounds* **2007**, *427*, 171-175.
57. Glade, S.C.; Johnson, W.L. Viscous flow of the Cu₄₇Ti₃₄Zr₁₁Ni₈ glass forming alloy. *J. Appl. Phys.* **2000**, *87*, 7249-7251.
58. He, S.; Liu, Y.; Huang, B.; Li, Z.; Wu, H. Effect of Zr on glass-forming ability and crystallization kinetics of Y₅₆Al₂₄Co₂₀ metallic glass. *J. Mater. Proc. Techn.* **2008**, *204*, 179-183.
59. Zheng, Q.; Xu, J.; Ma, E. High glass-forming ability correlated with fragility of Mg–Cu(Ag)–Gd alloys. *J. Appl. Phys.* **2007**, *102*, 113519:1-113519:5.
60. Busch, R.; Bakke, E.; Johnson, W.L. Viscosity of the supercooled liquid and relaxation at the glass transition of the Zr_{46.75}Ti_{8.25}Cu_{7.5}Ni₁₀Be_{27.5} bulk metallic glass forming alloy. *Acta Metall.* **1998**, *46*, 4725-4732.
61. Zhang, B.; Wang, R.J.; Zhao, D.Q.; Pan, M.X.; Wang, W.H. Properties of Ce-based bulk metallic glass-forming alloys. *Phys. Rev. B* **2004**, *70*, 224208:1-224208:7.
62. Bian, X.F.; Sun, B.A.; Hu, L.N.; Jia, Y.B. Fragility of superheated melts and glass-forming ability in Al-based alloys. *Phys. Lett. A* **2005**, *335*, 61-67.

63. Chen, H.; Turnbull, D.J. Evidence of a glass-liquid transition in gold-germanium-silicon. *J. Chem. Phys.* **1968**, *48*, 2560-2571.
64. Adam, G.; Gibbs, J.H. On the temperature dependence of cooperative relaxation properties in glass-forming liquids. *J. Chem. Phys.* **1965**, *43*, 139-146.
65. Turnbull, D.; Fisher, J.C. Rate of nucleation in condensed systems. *J. Chem. Phys.* **1949**, *17*, 71-73.
66. Cernosek, Z.; Holubova, J.; Cernoskova, E. Kauzmann temperature and the glass transition. *J. Optoelectron. Adv. Mater.* **2005**, *7*, 2941.
67. Cernosek, Z.; Holubova, J.; Cernoskova, E.; Liska, M. Enthalpic relaxation and the glass transition. *J. Optoelectron. Adv. Mater.* **2002**, *4*, 489-503.
68. Mehl, P.M. Determination of enthalpy relaxation times using traditional differential scanning calorimetry for glycerol and for propylene glycol. *Thermochem. Acta* **1996**, *272*, 201-209
69. Fransson, A.; Bäckström, G. Isothermal enthalpy relaxation of glycerol. *Int. J. Thermophys.* **1987**, *8*, 351-362.
70. Néel, L. Superparamagnétisme de grains très fins antiferromagnétiques. *C. R. Am. Sci.* **1961**, *252*, 4075-4080.
71. Wu, D.T.; Granasy, L.; Spaepen, F. Nucleation and the solid-liquid interfacial free energy. MRS Bulletin. Available online: <http://www.mrs.org/publications/bulletin> (accessed on December 2004).
72. Berton, A.; Chaussy, J.; Odin, J.; Rammal, R.; Tournier, R. Magnetocaloric investigation of (H,T) phase diagram of Cu-Mn spin glass. *J. Physique-Lett.* **1982**, *43*, L153-L158.
73. Tholence, J.L.; Tournier, R. Susceptibility and remanent magnetization of a spin glass. *J. Phys. Suppl. Coll.* **1974**, *35*, C4:229-C4:235.
74. Mydosh, J.A. *Spin Glasses: An Experimental Introduction*; Taylor & Francis: London, UK, 1993.
75. Mei, J.N.; Soubeyroux, J.L.; Blandin, J.J.; Li, J.S.; Kou, H.C.; Fu, H.Z.; Zhou, L. Structural relaxation of $\text{Ti}_{40}\text{Zr}_{25}\text{Ni}_8\text{Cu}_9\text{Be}_{18}$ bulk metallic glass. *J. Non-Cryst. Sol.* **2011**, *357*, 110-115.